Geomorphic Controls on Andean Denudation Rates

Rolf Aalto, Thomas Dunne,[1] *and Jean Loup Guyot*[2]

Quaternary Research Center and Department of Earth and Space Sciences, University of Washington, Seattle, Washington 98195, U.S.A.
(e-mail: aalto@u.washington.edu)

ABSTRACT

To predict erosion rates throughout the Andes, we conducted a multiple regression analysis of the sediment discharge from 47 drainage basins in the Bolivian Andes and various topographic, climatologic, and geologic parameters. These mountainous basins are typically large (17–81,000 km^2; mean = 11,000 km^2), often have decades of measurement data on daily water and sediment discharge, and display an extraordinary range of denudation (0.01–6.9 mm/yr), runoff (16–2700 mm/yr), and local topographic relief (700–4300 m), yet the underlying lithology (granitic plutons, metasediments, and Quaternary deposits) can be classified into a small number of homogeneous types, and anthropogenic disturbance is limited. The steep nature of the channels precludes sediment storage, and unlike previous global studies of fluvial denudation rates, based on data compilations from very large river basins (>100,000 km^2), this analysis distinguishes the sediment production in mountains from sediment entrapment within adjacent sedimentary basins. Lithology and average catchment slope account for 90% of the variance in sediment yield, and yield is not significantly correlated with runoff. However, because runoff over geologic timescales orchestrates the processes of channel network incision and sediment evacuation, climate could ultimately govern basin hillslope conditions and thereby the rates of hillslope erosion. Several theoretical geomorphic models for mass wasting are tested to assess hillslope-scale sediment yield models for the study basins. When applied throughout the Amazonian Andes, such empirical models predict an annual Andean sediment flux to the lowland Amazon Basin of 2.3–3.1 Gt. Because ~1.3 Gt/yr of sediment reach the gauged tributaries of the mainstem Amazon River, the intervening foreland basins appear to intercept about half of the total Andean sediment discharge.

Introduction

Since Ahnert (1970) published the first study of mountain basin denudation incorporating a parameterization for potential energy (local relief), numerous researchers have followed suit, each finding catchment sediment yield (discharge per unit area) proportional to some topographic index such as elevation, slope or relief, and basin area. Milliman and Meade (1983) cataloged sediment discharge from the major rivers of the world and noted that sediment yield strongly decreases with increasing drainage basin area. Pinet and Souriau (1988) analyzed an expanded version of this data set, which Milliman and Syvitski (1992) further supplemented with data from smaller basins in their assessment of total sediment discharge to the ocean. Summerfield and Hulton (1994) investigated a large-basin subset (areas >5 × 10^5 km^2) to ascertain morphometric controls on fluvial denudation rates; Hicks et al. (1996) investigated erosion in New Zealand basins, highlighting the influences of lithology and climate (runoff); and Hallet et al. (1996) compared rates of glacial erosion and sediment evacuation to the high mountain sediment yields defined by Milliman and Syvitski (1992). Recent studies by Ludwig and Probst (1998) and Hovius (1998) summarize much of this earlier work and provide extensive statistical analysis of the largest global database currently available.

These studies share three noteworthy geomorphic simplifications: (1) entire basins, regardless of size, are treated as homogenous units without considering whether they include internal zones of sed-

Manuscript received April 7, 2005; accepted July 21, 2005.

[1] Donald Bren School of Environmental Science and Management, Department of Geological Sciences, University of California, Santa Barbara, California 93106, U.S.A.

[2] Institut de Recherche pour le Développement–Unité Mixte de Recherche, Laboratoire des Mécanismes et Transferts Géologie, Université Paul Sabatier, 38 rue des 36 Ponts, 31000 Toulouse, France.

[The Journal of Geology, 2006, volume 114, p. 85–99] 0022-1376/2006/11401-0005$15.00

iment erosion, transport, and deposition; (2) the sediment discharge for most basins, large and small alike, is measured near the river's mouth, well downstream from any internal loci of deposition in the cases of the large basins; and (3) these studies focus primarily on large rivers, where such effects are greatest. Because larger basins tend to have more extensive low-gradient zones (cratonal shields, foreland basins, and other depocenters) compared to areas of high relief (active orogens, dissected uplands, and other sediment sources), basin area in most of these studies shows a significant negative correlation with denudation, runoff, and total sediment discharge. Because basin area itself has no apparent physical effect on erosion rate, it cannot have any direct causal relationship with sediment yield. Hence, the observed statistical relationships are likely to be artifacts of the ratio between sediment-producing area and depositional area (or length), which generally decreases with increasing basin size. By not distinguishing the zones of sediment production, transport, and deposition within basins, previous studies do not resolve realistic process rates within these distinct mesoscale geomorphic process zones. Rather, they provide an empirical basin-averaged proxy for the downstream area–integrated effects of erosion, transport, and deposition and consequently afford limited quantitative insight into the contribution of each specific geomorphic process. Because the spatial distribution of these mesoscale process zones varies considerably between basins, the common procedure of grouping all the rivers in a single type of topographic class under a single sediment yield area relationship is of limited value for understanding erosion and sediment transport, especially when these generalized logarithmic trends in whole-basin sediment yields are cited as empirical proxies for the rates of more localized geomorphic mechanisms.

To investigate the geomorphic controls on denudation rates in mountains, we select basins that are purely erosional in nature and conduct a multiple regression analysis of how sediment yields vary with topographic, climatologic, and geologic basin parameters. This analysis provides insights into the geomorphic controls on the processes and rates of sediment production for rugged mountainous catchments throughout Bolivia. Next, to investigate sediment delivery to lowland basins, we recast the empirical basin-scale analysis into a hillslope-scale, cell-based framework, which can be applied to estimate erosion-dominated sediment supplies elsewhere throughout the Andes.

Study Methods and Basins

Because of these problems arising from the increasing significance of deposition with larger basin area, we have identified a set of mountainous basins that are largely free of significant sediment sinks (Aalto et al. 1996). They are purely denudational basins, representative only of mesoscale, erosional geomorphic process zones. The absence of depositional zones was determined by extensive field inspection and from the absence of wide valley flats with meandering or braided channels on satellite images and 1 : 100,000-scale topographic maps. We were also concerned about whether sediment yields have been significantly perturbed by land use since European colonization. We examined erosion features (e.g., rilling, gullying, and landsliding), sediment sources, and local sediment storage on field surveys throughout the region and determined that soil erosion has been accelerated in a few cultivated regions, particularly near cities such as Cochabamba and Santa Cruz and, to a lesser extent, La Paz and Sucre (fig. 1). However, these areas are surrounded by even more impressive landslides and gullies throughout vast expanses of uninhabited terrain. Despite some dramatic, qualitative descriptions of soil erosion that imply anthropogenic effects, the first detailed studies are beginning to document only local and moderate rates of erosion resulting from land use (Preston 1998). Hence, it appears that the sometimes confounding effects of anthropogenic disturbance (Walling and Webb 1983; Milliman et al. 1987) and changes in floodplain sediment storage (Trimble 1976, 1977) are minimal within the study area and that the typically large basin size effectively averages much of the small-scale stochastic sediment supply from individual hillslopes, so the decadal-scale sediment yields reflect the rate of sediment delivery from hillslopes under the current climate conditions, which have been relatively stable for the last 1500 years (Servant and Servant-Vildary 2003).

The Bolivian Andes offer an excellent case study of erosion rates from a rugged mountain belt undergoing active crustal shortening (Norabuena et al. 1998) across a series of east-vergent, crustal-scale thrusts of the Subandean fold and thrust belt. Lithologies include arenites, argillites, lutites, and conglomerates of Paleozoic, Mesozoic, and Tertiary age, with a backbone of Mesozoic and Cenozoic granitic batholiths that form the peaks of the Eastern Cordillera Real and blankets of massive ignimbrites covering portions of the Andes east of the Altiplano. Drained by the Beni, Mamore, Grande, Pilcomayo, and Bermejo rivers, this region (fig. 1)

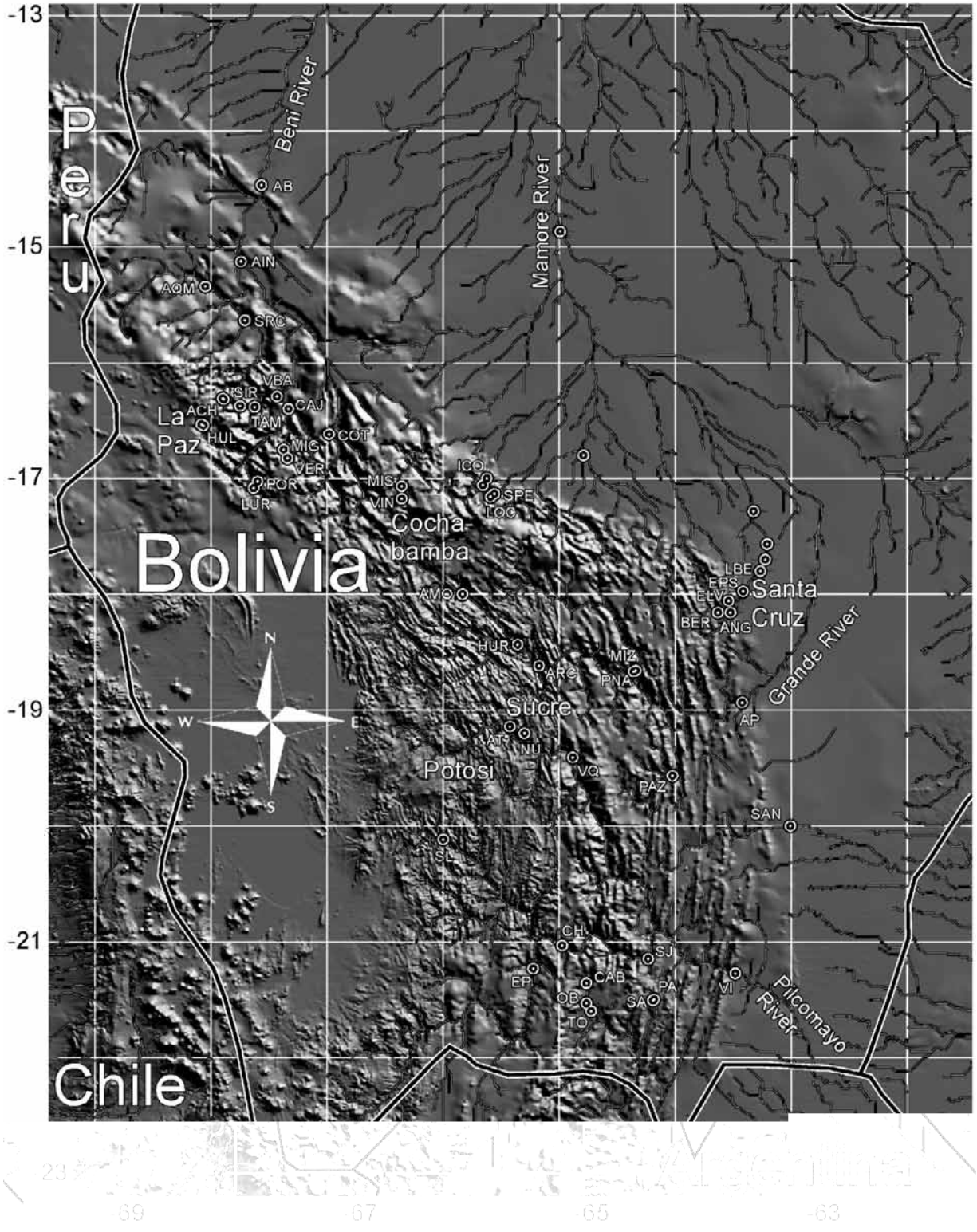

Figure 1. Shaded topographic map of Bolivia with marked gauging stations and digital elevation model rivers.

features substantial variation in lithology (granite to unconsolidated alluvium), basin relief (700–4300 m), average basin hillslope, average elevation (800–4700 m), runoff (16–2700 mm/yr), seasonality, and vegetation cover (0%–100%). Such an extraordinary range of parameters facilitates statistical identification of probable physical controls on mass wasting once catchments with sediment sinks are identified and excluded from the analysis. Quaternary glaciation was limited to the high peaks of the Cordillera Real, affecting only the highest, relatively minor regions of the Beni river basin.

Water and sediment discharge data (2–35 yr) were collected at >60 locations throughout Bolivia by several governmental and scientific organizations that utilized a variety of sampling techniques (e.g., daily surface grab samples, sediment concentration measurements correlated with river stage, and depth-integrated sediment discharge samples). At some stations, hundreds to thousands of samples were collected. The sediment concentrations have been combined with river flow measurements in various ways (daily totals, monthly totals) to produce average annual sediment fluxes. These data, along with measurements of basin morphometry, runoff, vegetative cover, lithologic index, and other geomorphic parameters, were augmented and collated by Guyot (1993) and Guyot et al. (1989*b*). Most of the flux estimates were based on surface-sampled suspended load and cannot be calibrated for the depth dependence of sediment concentration. However, at shallow river depths and steep Andean river gradients, the resulting underestimate of suspended sediment discharge should be relatively minor (5%–25%) for the majority of fine particles (Guyot 1993; Aalto 1995). Suspended load typically represents 85% (Guyot et al. 1990) to well over 90% of total solid flux (Collins and Dunne 1989) from large humid basins, although this figure may drop to 75%–80% for arid basins or small mountain catchments. Also, we are not accounting for solute fluxes (a few percent, according to Guyot [1993]), and the data we are analyzing were produced by various methods of combining concentrations and discharges that often produce lower estimates of flux (Walling and Webb 1981; Ferguson 1987). Therefore, these effects combine to systematically produce conservative estimates (10%–40% low) of the total mass removal from the study basins. As a first step, we culled those flux data from stations for which the sum of sediment inputs from gauged upstream stations greatly exceeded (>25%) the downstream load. Such discrepancies exceed measurement error and reflect significant sediment sinks, and all such stations were located downstream of the Andes in the foreland basins, where there is copious field evidence of extensive floodplain deposition (Aalto et al. 2003).

The GTOPO30 topographic database for Bolivia, a 30″ (~900 m) digital elevation model (DEM; Bliss and Olsen 1996), was used to perform basin-scale morphometric analyses (average elevation, average slope), to calculate an index of local steepness for the "hillslope-scale" flux models and for assisting with landscape visualization. While the scale of the DEM does not accurately represent topographic details, the dramatic relief and enormous valleys typical to the Bolivian Andes compensate in part for this coarse resolution. However, the degree to which the DEM provides only an index of the topography is indicated by the discrepancy between the average hillslope gradient measured from different topographic databases. The area-weighted average hillslope gradients (average slope "index," S_{avg}, calculated from a 3 × 3 DEM neighborhood using the average-maximum technique) derived from the 30″ DEM lie in the range of 2°–14°. A 25-m-resolution DEM obtained from the SIR-C shuttle mission for a representative high-relief basin (of the Zongo River, with a 1-km DEM average slope index [S_{avg}] of 10°) yields an average hillslope of 31°, a number much closer to our field measurements. Not only is the 30″ DEM vastly coarser than the 25-m DEM, but the corresponding DEM slope is further smoothed by using the standard average-maximum technique, which calculates the steepest descent of the best-fit plane within a 3 × 3 DEM neighborhood (therefore generating a "slope" DEM sampled at ~1800-m pixel resolution). Nevertheless, these 30″ elevation data provide a consistent means to quantify basin relief and an index of average slope over the large study area. Despite its systematic underrepresentation of average slope, the 900-m DEM is more reliable in estimating total basin relief. For each basin, we also determined an average mean local relief (the maximum elevation difference observed within a 5-km search radius of each measurement point, as defined by Ahnert [1970]), a value that should be largely independent of DEM resolution (Polidori et al. 1991; Montgomery and Aalto 2001).

We have also used 1 : 50,000 scale topographic maps of parts of the study area as well as the 25-m NASA SIR-C DEM (where available) and edited portions of the 1-km DEM to correct errors in the river network. From the corrected 900-m DEM, we generated longitudinal river profiles to identify reaches where channel gradient and hence sediment transport capacity decreases rapidly (e.g., large synclinal valleys in the Subandean fold and

thrust belt). These locations were then flagged as potential sediment sinks to be evaluated further with Landsat imagery and by field inspection for evidence of sediment storage. To evaluate potential sediment traps, we obtained spatially and temporally extensive Landsat TM and MSS satellite images spanning 1972–2000 for most of the study region, enabling evaluation of channel shifting, bar deposition, and other characteristics of active deposition over the last ~30 yr. Landsat band ratios and linear mixture analysis (Mertes et al. 1993) were used to classify Landsat pixels as water, vegetation, and active (unvegetated) gravel bars. Reaches with comparatively high rates of channel migration across a broad valley floor, extensive active bars, and substantial changes in slope were identified as potential sediment sinks. Stations downstream from these sinks may no longer represent purely erosional basins and were therefore flagged for further scrutiny. By measuring grain-size distributions and observing geomorphic processes in the field at many of these locations, we evaluated the significance of the suspected sedimentation. For example, we visited a large intramontane basin within the Beni River system every year for 4 yr to observe the morphology of channel bed and floodplain deposition, ultimately deciding that the observed gravel bar deposition across the valley is only a few meters deep (and is constantly reworked with no apparent aggradation) and amounts to only a small fraction of the total sediment flux. We then made rough estimates of the magnitude of sediment deposition within these sinks, discarding stations with substantial upstream deposition. After a lot of searching, image interpretation, field inspection, storage analysis, and discussion, ultimately, because of the narrow valleys, steep channels, and high sediment fluxes, only two Andean stations were discarded. Both of them were in small, recently deglaciated catchments with low sediment yields, where clasts generated by hillslope failures accumulate primarily as talus at the bottom of the cliffs, distant from the active channel in the center of these classic glacial valleys. Our field inspection and image analysis of erosion processes throughout the Beni River basin suggest that deposits of loose material produced by Quaternary glaciation do not significantly contribute to modern sediment yields in the Beni; such stores may have previously been evacuated during deglaciation, leaving only small remnants that are of little significance within large, rapidly eroding basins. In all but one of the arid southern rivers, there is no obvious mobilization of previously stored sediment—the exception to this rule, the Grande River, will be discussed later. The sediment loads of all stations within or downstream of the foreland basin are affected by extensive upstream deposition and were therefore discarded. Thus, the data set contains no major sediment sinks and represents hillslope erosion processes. We can utilize such "erosional" discharge stations for our statistical analysis of present-day Bolivian denudation rates.

We defined the lithology of each study basin by digitizing a 1 : 1,000,000-scale geologic map of Bolivia (Pareja and Ballón 1978). To document the range of rock strength quantifiable at the small scale, we measured the compressive rock strength of lithologies at 50 sites using a Schmidt hammer (table 2) and made field observations of the associated morphology of mass wasting. These measurements correlated with the lithologic index that Probst (1990) developed to classify rock types according to their susceptibility to chemical weathering (tables 1, 2) as estimated by Meybeck (1987). We next used a weighted-area-averaging routine in a geographic information system (GIS) to generate an area-weighted Probst lithologic index (PLI) for each basin (table 1) and then grouped the study basins by this average value into one of three distinct lithologic classes: igneous, metasedimentary, and weak sedimentary rock. Basins dominated by the batholiths and ignimbrites (and possibly containing some metasedimentary rock) have average PLI values from 1.0 to 4.0, which we group as "igneous" and are typically found in the high Andes. Most of the lower, larger Andean and Subandean basins contain mixtures of metasedimentary and weak sedimentary rocks and have average PLIs from 4.0 to 12.0, which we group as "metasedimentary." Some Subandean basins contain considerable expanses of Plio-Pleistocene fanglomerates, river and floodplain deposits, and other weakly consolidated strata and have average PLIs greater than 12.0, which we group as "weak sedimentary." The average PLI discriminating value at 4.0 is physically based, representing the transition to basins without extensive igneous rocks. However, the transition at 12.0 was selected based on obtaining the best separation of the metasedimentary and weak sedimentary data clouds—we discovered that basins containing even small areas of unconsolidated alluvium or colluvium had exceptionally high erosion rates.

Basin Sediment Yields

The 47 sink-free Andean basins exhibited average erosion rates of 0.01–6.9 mm/yr (table 1). The data were entered into a forward stepwise multiple re-

Table 1. Bolivian River Gauging Stations without Major Sediment Sinks, Including Most of the Morphologic Parameters Used in the Regression Analysis

Station code	Basin area (km^2)	Station altitude (m)	Avg. annual discharge (m^3/s)	Avg. altitude (m)	Avg. slope (deg.)	Avg. local relief (m)	Max. DEM relief (m)	Trunk stream length (km)	Relief ratio (m/m)	PLI	Assigned lithologic class	Soil carbon (t/ha)	No. concentration measurements	Runoff (mm/yr)	Sediment flux (Mt/yr)	Yield ($t/km^2/yr$)	Basin denudation rate (mm/yr)
SIR	270	1640	12	3565	13.7	1815	3235	40	.080	3.8	Igneous	89	194	1400	2.0	7420	2.80
TAM	950	1185	52	3561	13.1	1826	3862	56	.069	3.6	Igneous	71	320	1730	2.4	2520	.95
VBA	1900	1050	67	2937	11.8	1621	4172	85	.049	3.8	Igneous	75	353	1110	7.8	4110	1.55
HUL	17	3620	.1	3922	6.0	1113	1048	10	.108	30.0	Weak sed.	5	349	190	.069	4060	1.53
ACH	38	3580	.2	4188	7.4	1124	1345	12	.113	34.0	Weak sed.	7	131	170	.2	5300	2.00
LUR	810	2550	10	4053	5.0	780	2366	56	.042	15.4	Weak sed.	9	39	390	6.4	7910	2.98
POR	240	2500	3	4065	8.5	1256	2143	26	.083	6.2	Metased.	11	36	380	.8	3310	1.25
VER	140	2830	5	4729	5.0	930	1818	23	.080	2.0	Igneous	14	146	1130	.011	80	.03
MIG	360	1980	17	4284	7.8	1232	2693	34	.080	2.0	Igneous	37	87	1490	.047	130	.05
CAJ	6500	760	99	3498	9.3	1332	4214	159	.027	14.0	Weak sed.	30	332	480	119.0	18,310	6.91
COT	5600	1270	84	3389	9.7	1355	4299	148	.029	4.2	Metased.	24	105	470	40.6	7240	2.73
MIS	350	3700	4	4264	5.3	724	920	26	.036	4.0	Igneous	9	153	400	.012	30	.01
VIN	50	3700	1	4442	5.2	802	676	9	.076	4.0	Igneous	8	1141	510	.003	60	.02
LOC	200	1700	15	3121	12.3	1838	3133	23	.136	3.9	Igneous	47	1000	2370	.67	3350	1.26
SPE	320	1040	27	2921	12.0	1836	3576	28	.126	5.7	Metased.	59	190	2660	3.5	10,940	4.13
ICO	2300	600	130	2556	8.3	1248	3974	87	.046	5.1	Metased.	84	186	1780	11.4	4960	1.87
BER	480	900	4	1491	4.6	582	1229	39	.031	4.6	Metased.	184	2220	280	.60	1250	.47
ANG	1420	650	11	1462	4.3	574	1798	72	.025	4.4	Metased.	177	3027	240	2.9	2040	.77
ELV	64	650	1	1247	5.7	860	1025	13	.077	4.8	Metased.	182	2162	250	.03	470	.18
EPS	203	550	3	883	3.6	532	1046	25	.043	12.6	Weak sed.	209	2186	400	.42	2070	.78
AMO	9200	1850	59	3304	5.7	834	2927	170	.017	14.0	Weak sed.	10	580	200	126.1	13,700	5.17
HUR	11,200	1600	70	3589	7.6	948	3334	258	.013	5.0	Metased.	10	282	200	14.1	1260	.48
ARC	23,700	1500	130	3314	6.9	911	3511	300	.012	6.8	Metased.	13	868	170	154.3	6510	2.46
PNA	31,200	950	220	3059	6.7	901	4024	428	.009	6.1	Metased.	19	938	220	206.9	6630	2.50
MIZ	10,800	950	47	2390	5.1	742	3544	247	.014	4.6	Metased.	32	897	140	14.1	1310	.49
PAZ	4360	1080	32	2200	5.3	789	3061	151	.020	6.2	Metased.	57	557	230	2.2	510	.19
SAN	7500	550	79	1264	3.2	484	2705	228	.012	18.8	Weak sed.	127	642	330	19.4	2590	.98
AT	6340	2500	20	4021	5.5	764	2565	186	.014	5.6	Metased.	7	1088	98	12.0	1890	.71
NU	1600	2300	8.5	3497	7.7	954	2231	95	.024	7.3	Metased.	6	46	168	1.1	690	.26
VQ	13,200	2000	49	3644	5.9	809	3164	269	.012	6.6	Metased.	6	552	117	22.0	1670	.63
SL	4200	3100	6.5	4064	5.2	696	2272	113	.020	4.0	Igneous	10	57	49	.50	120	.04
EP	20,100	2300	10	3870	3.6	557	3420	389	.009	10.8	Metased.	8	584	16	2.4	120	.05
CH	42,900	2100	53	3734	4.5	649	3734	453	.008	7.5	Metased.	8	549	39	14.0	330	.12
SJ	47,500	800	82	3646	4.8	688	4977	563	.009	7.2	Metased.	10	309	54	31.0	650	.25
VI	81,300	340	260	3263	5.2	739	5441	697	.008	6.9	Metased.	22	745	99	72.0	890	.33
CAB	230	2100	1.5	2801	4.7	734	1319	27	.049	5.4	Metased.	7	444	206	.05	220	.08
OB	920	1900	3.8	2653	5.1	803	2263	47	.048	12.0	Metased.	10	192	130	.40	440	.16
TO	460	1900	9	2594	7.0	1148	2805	36	.078	12.0	Metased.	11	584	617	1.5	3261	1.23
SA	290	1200	5.9	2214	4.4	701	1700	35	.049	4.4	Metased.	44	181	642	.06	207	.08
PA	220	1200	4.6	2068	5.3	860	2143	34	.063	4.6	Metased.	72	182	660	.11	500	.19
AQM	9400	500	420	2678	4.3	734	5294	147	.036	14.0	Weak sed.	80	351	1410	36.8	3900	1.47
SRC	4700	440	260	2212	7.8	1142	5052	125	.040	3.8	Igneous	106	49	1750	7.1	1500	.57

Table 2. In Situ Measurements of Compressive Rock Strength with the N-Type Schmidt Hammer at 51 Sites throughout Bolivia, Providing an Estimate of the Local-Scale Strength of Unfractured, Unweathered Rock Samples

	Compressive strength (n mm^{-2})	Assigned PLI
Igneous:		
Granite	80 ± 14	1
Ignimbrite	51	2
Metasedimentary:		
Quartzite	83 ± 7	4
Slate	77 ± 4	4
Schist	63 ± 14	4
Strong sedimentary:		
Massive sandstone	51 ± 10	4
Massive greywacke	54 ± 9	4
Weak sedimentary:		
Greywacke	19 ± 6	10
Phyllite	23 ± 5	10
Weathered sandstone	7 ± 2	10
Unconsolidated:		
Colluvium and alluvium	0	40

Note. Averages and standard deviations of six to 10 impact measurements (corrected for hammer orientation) at each location. The Probst lithologic index (PLI), which represents the relative rates of chemical erosion observed for each rock type (Probst 1990), has been assigned to each major lithology (Guyot 1993; this study), with the basin-averaged values reported in table 1. For this analysis, the "strong sedimentary" lithologic class (common throughout the Andes) is combined with the "metasedimentary" group, which occurs within the major valley bottoms and therefore probably extensively at depth within the mountains, although it is of more limited spatial extent higher on the valley walls). This new group is henceforth referred to as "meta-seds" and is assigned a common PLI of 4.

gression analysis (tol = 0.05, F statistic = 2.0) to determine statistically significant controls of average annual basin sediment flux (Mt/yr). Of the tested parameters (table 3), area (A), lithology (average PLI in table 1), and average slope index (S_{avg}) were found to be statistically significant (in log-linear space) and were therefore selected for further analysis. Data from the three general lithologic classes define subparallel lines when basin sediment flux per unit area (yield) is plotted against S_{avg} (fig. 2A). Mean local relief can effectively replace average slope index in this relationship (fig. 2B), although the explained variance declines considerably. While this mean local relief relationship is probably more transportable between DEMs of varying resolution and quality, for the purposes of this study (which uses a consistent DEM for all analysis), we will focus on the better statistical relationship for the S_{avg}.

To elucidate the contribution of rock strength in determining average basin erosion, it is useful to (1) assume that the best-fit lines associated with the igneous and weak sedimentary lithologic groups actually have the same slope as the largest metasedimentary group because their regression slopes are not statistically different, (2) fit the intercepts for these parallel lines through each data set to minimize variance, and then (3) compare the ratio of their intercepts, thereby deriving a relative lithologic index of erosion (L). For the mean slope relationship, the observed ratio (fig. 2A) of 46 : 7.2 : 1, once the slopes are fixed (at the slope of the intermediate class, which has the largest sample size and the best-defined regression), expresses the expected increase in sediment production for basins composed of weak sedimentary and strong sedimentary rocks as compared with granitic basins of the same average hillslope, accounting for 77% of the variation in yield. In Bolivia, lithologic variation accounts for an observed 46-fold range in sediment yields. In situ compressive strength varies over a factor of ~4 for fresh rock (table 2), so the geomorphic processes of erosion apparently augment these simple material strength differences by approximately an order of magnitude.

We use the fitted relationship of sediment flux to S_{avg} and lithology (L) depicted in figure 2A to normalize sediment discharge and plot this flux versus basin area in figure 2C. An almost exactly linear function of basin area emerges, as would be expected if the role of basin size was simply that of a passive scaling factor without any direct mechanical effect on erosion, sediment transport, or storage. In this way, we separate the effect of basin size out of the calculation of sediment production per unit area of an eroding continent; other analyses of sediment delivery to the ocean (e.g., Milliman and Syvitski 1992; Summerfield and Hulton 1994) incorporated nonlinear functions of basin size that therefore should not be applied to eroding landscapes without internal sediment sinks.

Table 3. Pearson Correlation Matrix for the Log Values of Parameters Depicted in Table 2

	Basin area (km^2)	Station altitude (m)	Avg. annual discharge (m^3/s)	Avg. altitude (m)	Avg. slope (deg.)	Avg. local relief (m)	Max. DEM relief (m)	Trunk stream length (km)	Relief ratio index (m/m)	PLI	Soil carbon (t/ha)	Runoff (mm/yr)	Sediment flux (Mt/yr)
Station altitude (m)	−.48												
Avg. annual discharge (m^3/s)	.85	−.62											
Avg. altitude (m)	−.01	.71	−.04										
Avg. slope (deg)	−.16	.22	.14	.51									
Avg. local relief (m)	−.25	.26	.08	.54	.98								
Max. DEM relief (m)	.78	−.45	.88	.15	.32	.29							
Trunk stream length (km)	.99	−.49	.82	−.04	−.19	−.29	.76						
Relief ratio (m/m)	−.90	.40	−.60	.15	.46	.57	−.45	−.92					
PLI	.07	−.13	−.12	−.25	−.39	−.35	−.05	.10	−.18				
Soil carbon (t/ha)	.02	−.79	.29	−.78	−.08	−.10	.12	.02	.04	−.11			
Runoff (mm/yr)	−.37	−.17	.16	−.03	.55	.62	.10	−.42	.64	−.34	.46		
Sediment flux (Mt/yr)	.85	−.50	.84	−.02	.14	.05	.83	.84	−.66	.24	.10	−.12	
Yield ($t/km^2/yr$)	.17	−.25	.35	−.03	.48	.46	.46	.17	.04	.35	.17	.30	.66

Note. Sediment yield is most strongly correlated with average slope and lithology (Probst lithologic index [PLI]). Other relevant parameters (e.g., runoff) are no longer significant once the first independent variables have been incorporated into the multiple regression analysis. DEM = digital elevation model.

Geomorphic Controls on Modern Sediment Yield

Of all the variables that we examined, topographic steepness and lithology appear to exert the strongest effect on basin-averaged erosion rate, as would be reasonably interpreted from current knowledge of hillslope erosion mechanics (Carson and Kirkby 1972) and empirical studies of river channel incision. While it may appear unusual that runoff (or rainfall) is not statistically related to denudation rate, several yield studies have reached similar conclusions (Ahnert 1970; Pinet and Souriau 1988). Comparison of erosion rates for seven small Sierra Nevada catchments, as estimated for the last few thousand years using cosmogenic nuclides, yielded a similar result (Riebe et al. 2001). Even the classic studies of climatic effects on sediment yield by Langbein and Schumm (1958) and Fournier (1960) proposed nonmonotonic relationships of undocumented statistical power between sediment yield and rainfall statistics, and there was no control of the results for the potential effects of topography or lithology. Other studies that have documented a relationship between denudation and runoff (Milliman and Syvitski 1992; Summerfield and Hulton 1994) have analyzed fluxes from large basins ($>5 \times 10^5$ km^2) and consequently suffer from the divergence between erosion rate and sediment yield that occurs in large basins, which tend to have greater areas of low relief and strong differences in runoff production. Besides serving as sediment sinks, these low-relief, low-gradient areas lack the higher orographic precipitation of mountainous regions, and some of the large interior basins in the data sets are distant from oceanic moisture sources. As a result, the aforementioned erosion studies find that runoff decreases significantly with increasing basin area, demonstrating how an increasing fraction of lowlands in a basin imbues the area parameter with a spurious physical significance, confounding the effects of rainfall and denudation rates. Because sediment yield also decreases with increasing basin area (Milliman and Syvitski 1992), it usually follows that in such global data sets, sediment yield increases with runoff because both increase together with decreasing basin area. For example, the Andes represent only 10% of the total Amazon basin area, yet they supply almost all of the sediment; in contrast, lowland Amazonia contains mostly sediment sinks, irrespective of rainfall (Dunne et al. 1998). Hence, while the effects of basin area may be ignored in some cases to provide simple estimates of total sediment discharge to the oceans from river mouths, the resulting statistical relationships are not causal and cannot be applied elsewhere because this apparent "area effect" probably scales differently between basins.

At first glance, it is perplexing that this and some other studies have found denudation rates statistically uncorrelated to runoff or rainfall. All geomorphic models of erosion, sediment transport, and fluvial landscape evolution are driven by the kinetic energy of rainfall and runoff (Carson and Kirkby 1972), as are simulation models based on stream-power-driven channel incision and sediment transport (Tucker and Slingerland 1994) or precipitation-driven surface erosion and mass failure (Chase 1992; Masek et al. 1994). However, given the enormous variation in runoff (17–2660

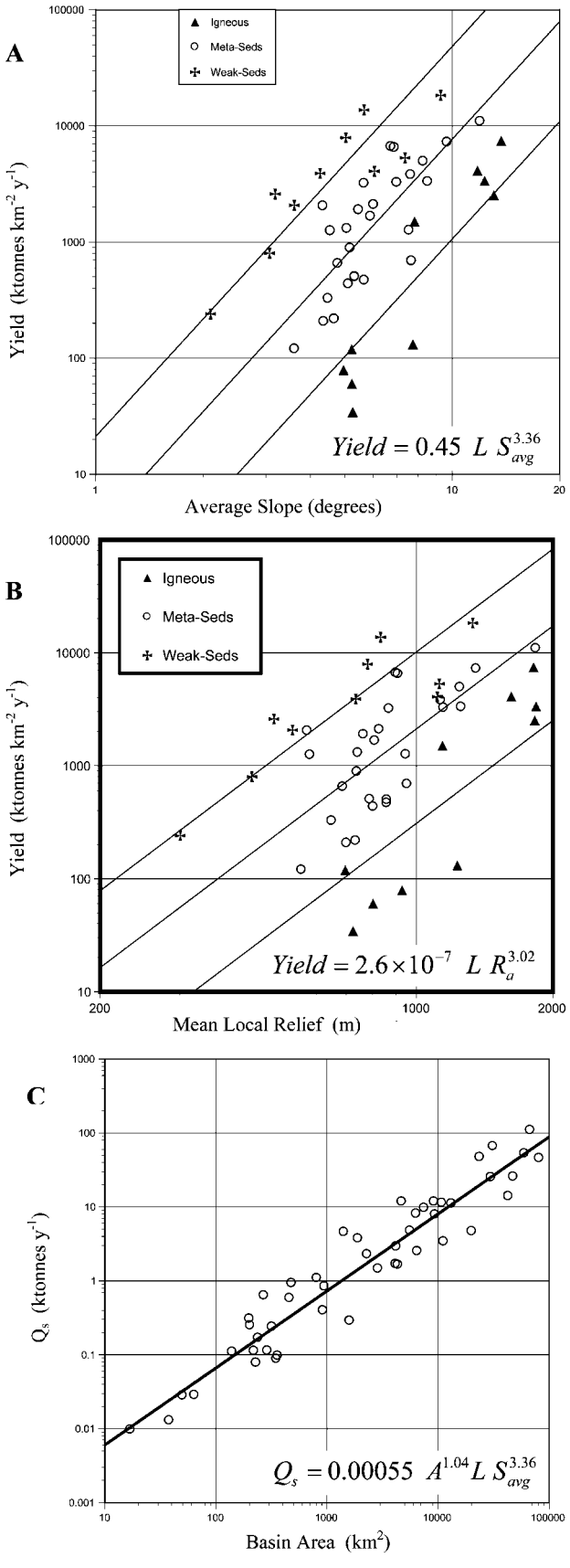

mm/yr), which should directly scale the stream power (per unit contributing area) throughout a channel network, and in sediment yield (34–18,300 t/km^2/yr), it is evident that annual runoff and sediment yield are only weakly correlated in the Bolivian Andes (fig. 3*A*). We have also regressed sediment yield against a measure of the wettest 3-mo seasonal concentration of rainfall without finding a significant correlation. In the multiple regression analysis, the variance in sediment yield explained by runoff is more strongly correlated with S_{avg}, due in part to the fact that runoff and average hillslope angle are correlated (fig. 3*B*). The fact that slope captures far more variance in sediment yield than does runoff or rainfall but that slope and runoff are weakly correlated precludes the recognition in a

Figure 2. *A*, Plot of basin yield versus average basin slope (S_{avg}) for the 47 Andean study basins, with basins classified according to their geographic information system–averaged Probst lithologic index (PLI, table 1). Slopes for the weak sedimentary ($n = 10$) and igneous ($n = 10$) lithologic groups were similar (at $P = 0.04$) to that for the larger meta-seds ($n = 27$) group ($P = 0.09$ and 0.04), so all were fitted with the slope of the metasedimentary group (3.36 ± 1.13, $P = 0.05$) to facilitate comparison of the intercepts (0.45 + 1.93/–0.37, 3.29 + 13.0/ − 2.63, and 20.6 + 63.5/ − 15.6; $P = 0.05$). The ratio of intercepts for each lithologic class defines a new lithologic erodibility index (L) with values of 1 : 7.2 : 46, respectively, for the igneous, metasedimentary, and weak sedimentary groups. Best-fit lines for igneous, metasedimentary, and weak sedimentary lithologic classes have respective R^2 values of 0.72, 0.67, and 0.55 ($P < 0.001$ for all). *B*, Plot of basin yield versus average local relief (R_a) for the study basins, classified according to their geographic information system–averaged PLI (table 1). Slopes for the smaller groups were again similar to that for the larger metasedimentary group ($P = 0.16$ and 0.03, respectively), so all were fitted with the slope of the metasedimentary group (3.02 ± 1.28, $P = 0.05$) to facilitate comparison of the intercepts (2.60E-7, 1.79E-6, and 8.57E-6). Ratio of intercepts for each lithologic class defines a slightly different lithologic erodibility index than in *A*: 1 : 6.9 : 33. Best-fit lines for igneous, metasedimentary, and weak sedimentary lithologic classes have respective R^2 values of 0.56, 0.49, and 0.49 ($P < 0.01$ for all). *C*, Plot of area versus study basin flux normalized (per the depicted equation) to the explained lithologic and slope variance as depicted in *A* (e.g., basin fluxes are divided by a factor of 1, 7.2, and 46 for igneous, metasedimentary, and weak sedimentary basins, respectively, a similar normalization is made for average slope, and the resulting flux is regressed against basin area). Best-fit line has slope 1.04 ± 0.096, and $R^2 = 0.92$ ($P < 0.00001$).

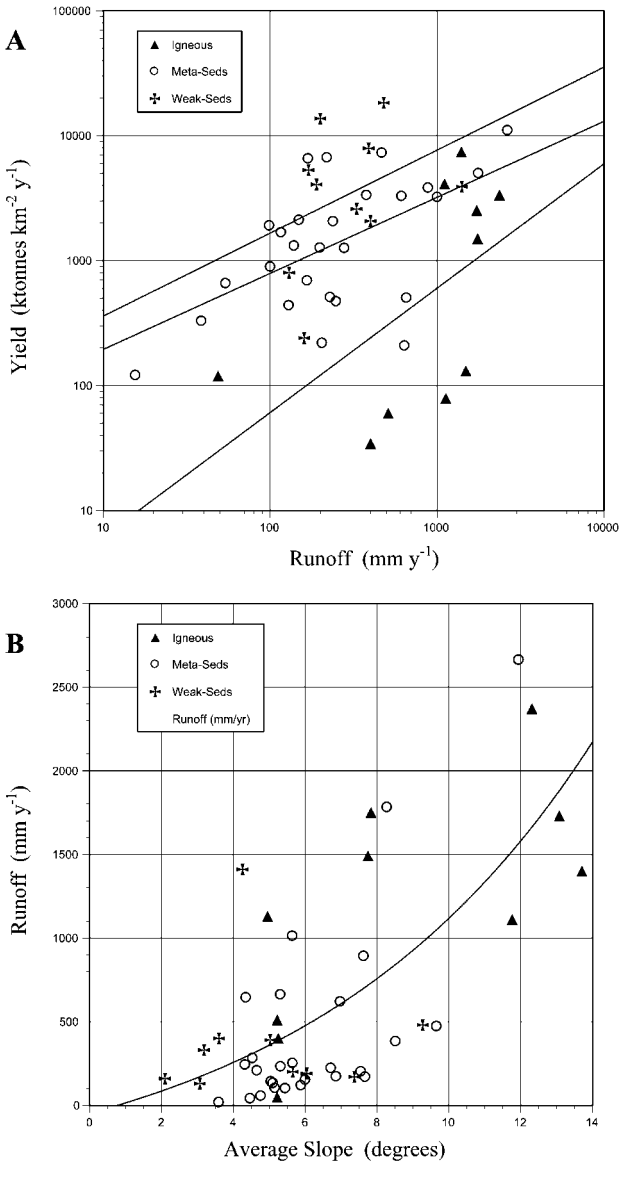

Figure 3. *A*, Relationship between annual runoff and erosion rate for all 47 study basins, showing a weak correlation. Best-fit lines for igneous, metasedimentary, and weak sedimentary lithologic classes have respective R^2 values of 0.31, 0.32, and 0.13 ($P = 0.047$, 0.001, and 0.15). *B*, Relationship between rainfall and average slope index (S_{avg}). Best-fit exponential curve to entire data set has $R^2 = 0.50$ ($P < 0.001$).

multiple regression analysis of any association that might exist between runoff and sediment yield. However, the product of runoff and S_{avg}, a measure of the energy expenditure rate of discharge similar to that used by Finlayson et al. (2002), does not offer a statistical improvement over slope index in explaining erosion. We are therefore challenged to explain the influence of climate on sediment yields that range well over an order of magnitude higher than those in classic sediment yield studies (Langbein and Schumm 1958), while stations in the drier Grande River basin of Bolivia, where erosion occurs by surface wash, deep gullying, and mass wasting, exhibit a range of erosion rates similar to those in the wettest part, the Beni basin (Guyot et al. 1989*a*), where erosion is dominated by mass wasting, including very large rockslides and deep gullies.

We propose several possible explanations for not recognizing a climatic effect, if in fact one exists. The first is that any effect of runoff on sediment yield may be nonmonotonic. However, we have no a priori basis for proposing a nonmonotonic regression model, as suggested by the data of Langbein and Schumm (1958) and Fournier (1960), for such a steep mountainous landscape with deep gullies and active mass wasting. The second possibility is that the steepest parts of our study area in the humid Beni River drainage basin may have attained steady state rates of river incision and hillslope mass wasting, which are in long-term topographic equilibrium (Montgomery 2001; Willett and Brandon 2002) with local uplift rates the result of the attainment of critical basin relief and failure threshold hillslopes (Schmidt and Montgomery 1995; Burbank et al. 1996, 2003; Montgomery and Brandon 2002). In such steep mountain valleys, bedrock landsliding produces a rate of exhumation approximately equal to the tectonic input regardless of regional variations in rainfall (i.e., a dynamic equilibrium exists between landslide frequency and magnitude, paced by river incision, such that there is no change in the average surface elevation). However, while such a steady state argument may be made (as discussed and modeled by Safran [1998]) for many of the 16 stations within the Beni basin, which has undergone rapid uplift and exhumation, few of the 31 other stations farther to the southeast seem likely to have reached any similar sort of dynamic equilibrium between tectonics and erosion (the Grande River basin in particular has high modern rates of erosion and steep slopes but low rates of uplift and runoff). The third possibility is that the climatic effect is simply obscured by the correlation between rainfall and average basin slope, to which erosion rate is particularly sensitive. Thus, in a stepwise multiple regression analysis, there is little residual variance that can be related to the precipitation variable once steepness has accounted for a majority of the total variance. We do not find any strong runoff-erosion relationship similar to the correlation that Hicks et al. (1996) found for mountainous New Zealand basins with similar

lithologies (although rainfall in that data set ranged up to 11,200 mm/yr, and their correlation between runoff and average hillslope angle is also highly significant). In conclusion, we cannot dismiss the importance of precipitation as a control on mountain erosion rates, but the effect does not appear to be straightforward and may not be as strong as the simple linear sensitivity incorporated into current landscape evolution models.

Potential Landscape Adjustment to Climate

The relation of erosion to average slope index (fig. 2) and the positive correlation between runoff and average slope index (fig. 3*B*) are intriguing because they suggest several possible feedback mechanisms over geologic time between higher precipitation and valley formation. First, more rain would imply a higher erosive stream power, favoring more intense channel network incision and the resulting excavation of deep valleys with steep, rapidly eroding hillslopes. Second, such large valleys could then convey moisture farther into the Andes and create macroscale atmospheric turbulence to enhance orographic precipitation—such a hypothesized condition appears to exist in the Beni River basin.

The reason that wetter landscapes have steeper slopes (fig. 3*B*) might be that runoff conditions could play a role in adjusting a landscape over geologic timescales via enhanced or diminished rates of channel network incision that determine the average basin hillslopes—the resulting mass wasting processes in turn control sediment delivery to the channels (e.g., incision rates decrease with runoff, decreasing average basin hillslope, and consequently the rates of denudation). In the extreme case of "fossilized" desert basins (represented in our data set by the two stations having runoff <40 mm/yr), the stream power of water is greatly reduced, and the sediment conveyance capacity of the channel network during floods may be insufficient to clear the bed of material supplied by soil production and hillslope mass wasting, exposing the underlying bedrock to abrasion. In the most arid regions of southeastern Bolivia, we have observed that many channels and valley floors are completely mantled by sediment that prevents or retards the further incision of the channel network into bedrock (Gilbert 1877). In contrast, the bare bedrock channels of the Beni River basin (and to a lesser degree the Grande and wetter portions of the Pilcomayo) have both excess transport capacity and a copious supply of large bedload clasts that can rapidly erode exposed channel bottoms (Sklar and Dietrich 2001). Hence, over geologic time, transport-limited desert basins would be expected to develop low sediment yields, caused by (1) low rates of sediment evacuation and channel network incision and (2) the resulting low-angled hillslopes with deep soils. This condition implies an end-member response of erosion to decreasing runoff, where the very driest landscapes have adjusted to contain sediment-armored channels with limited bedrock incision and flanked by stable, low-angle hillslopes with very little sediment production. As a result of such an arid climate sustained over geologic timescales, total exhumation and tectonic deformation in the Pilcomayo basin have been very low, leading to a substantial increase in the width of the Andean orogen (Gubbels et al. 1993; Horton 1999; Montgomery et al. 2001).

In conclusion, while climate does not show a strong statistical significance in predicting modern erosion rates in Bolivia, over geologic timescales it may play a key role in orchestrating the efficient sediment evacuation and bedrock abrasion necessary to maintain high rates of channel network incision. Thus, climate could affect the basin-scale rates of channel network incision that govern basin relief and average hillslope, which in turn determine the geomorphic processes and rates of mass wasting.

Cell-Based Models for Hillslope Erosion

To estimate erosion in Andean basins outside of our sample, we developed a flux model that estimates erosion based on the lithologic index (L) and the frequency distribution of hillslope angles within a basin. The hillslope angle is measured at the scale of 1–3 DEM pixels (1–3 km), as described earlier. Previous articles have proposed landscape evolution models that calculate erosion from a landscape cell as power, exponential, or threshold functions of local slope (e.g., Kirkby 1987; Howard 1994; van der Beek and Braun 1999). Granger et al. (1996) found that an exponential function of the average hillslope gradient best describes erosion rates within a small catchment. Accordingly, we tested various empirical models against basin sediment fluxes from all of our Bolivian basins for which the annual runoff exceeds 100 mm/yr (41 basins, after discarding six exceptionally arid basins from southern Bolivia that were mantled by sediment). We examined statistical models of the form shown in table 4, part B.

For all parameter values (variable n, table 4, pt. B, tested between 0.1 and 20.0 in steps of 0.1), versions of each flux model were applied on a cell-by-cell basis throughout the DEM and then summed

for each study basin. Values of the parameter L for average basin lithology were set to 46, 7.2, or 1, as derived from the foregoing analysis. After thus controlling for lithology, we regressed the "slope" function against observed sediment flux to determine which n and k best explained the observed variance in sediment discharge. Both models yield similar R^2 values (table 4, pt. B). Because pixel size is ~900 m, the valley-averaged "slope index" is not the actual angle of the local hillslopes where mass failures occur. Thus, despite the impressive scale of Bolivian hillslopes (often several kilometers), it seems problematic to apply a threshold failure model to a DEM of this resolution because (1) pixel scale is almost always larger than failure scale, and (2) without maximum slope values accurately observed at the failure scale, the selection of an appropriate S_{max} is somewhat arbitrary. Until we can utilize a higher-resolution DEM and lithologic data set for the Andes, simple power and exponential functions of slope appear to be the simplest candidates for a general mass-flux model applicable throughout the Amazonian Andes. Given previous work that estimates an annual Andean sediment input of at least 1.3 Gt much farther downstream into the lower main stem Amazon River (Dunne et al. 1998), it is interesting to estimate the total sediment efflux from the Andes to the Amazon basin. Lacking the necessary geologic maps to determine lithologic index for the entire Andean range, we employed the best-fit power and exponential equations for mass flux (fig. 4; table 4, pt. B) for an estimated range of average L values from 7 to 9 ($L = 8$ is the average for Bolivia). When the GIS procedure is applied to the 900-m DEM throughout the Amazonian Andes, these equations generate flux estimates of 2.3–3.1 Gt/yr to the range front, depending on which equation and constant L value is chosen. Evidently, the intervening foreland basins along the Andean range front intercept approximately half of the total mass flux out of the Andes, a fraction similar to that measured for the foreland basins of Bolivia (Guyot 1993; Aalto 2002). Because water surface measurements of suspended-sediment concentration used for this study underestimate total sediment flux, the best-fit equations and flux calculations represent conservative estimates. Dunne et al. (1998) utilized depth-integrated

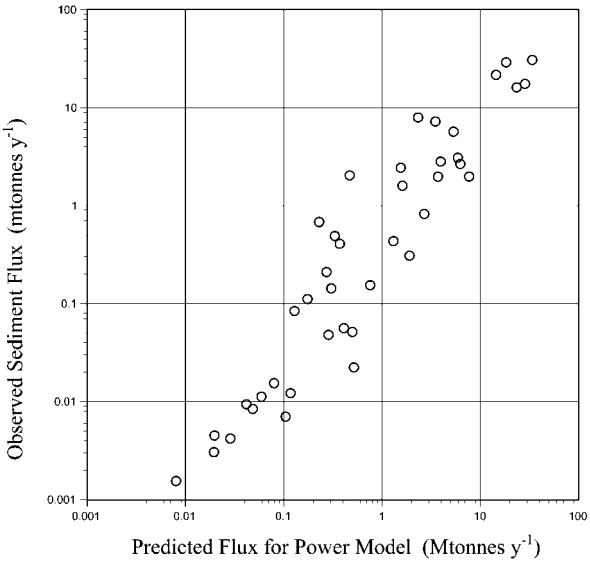

Figure 4. Plot of predicted versus observed sediment flux for the 41 study basins for which the annual runoff exceeds 100 mm/yr, the results of the digital elevation model cell-based power law depicted in table 4, part B. As listed in table 4, part B, $R^2 = 0.82$ ($P < 0.001$).

Table 4. Results of a Forward Stepwise Multiple Regression of Basin-Averaged Parameters and Cell Flux Models Tested for All Values of n between 0.1 and 20.0 for 41 Basins, Excluding the Six Most Arid Basins in Table 2

	Units	R^2
A. Multiple regression analysis for basins:		
Yield = $0.46\ L\ S_{avg}^{3.36}$	t/km^2/yr	.77
$Q_S = 0.00055\ A^{1.04} L\ S_{avg}^{3.36}$	Mt/yr	.92
B. Cell-based flux models applied to DEM:	Best k, n	R^2
$Q_S = \Sigma k S^n$	.0115, 1.6	.82
$Q_S = \Sigma k(e^{ns} - 1)$	.00076, 3.6	.81
$Q_S = \Sigma k\left(\frac{1}{S_{max} - S^n} - \frac{1}{S_{max}^n}\right)$	.0071, 3.7	.81

Note. In A, independent variables are listed in order of statistical significance. In B,negative terms for the exponential and threshold models are to force a zero flux for zero slope. Variables include average annual sediment discharge (Q_s), lithology (L), basin area (A), and average basin slope (S_{avg}, in degrees). For the flux models in pt. B, digital elevation model cell-based slope (S) is measured in units of gradient (m/m), not degrees, and sediment flux has been normalized to $L = 1$, the hypothetical flux for granite (e.g., before regression analysis, the recorded sediment fluxes from basins of metasedimentary and weak sedimentary lithology are reduced by factors of 7.2 and 46, respectively, and must therefore be reinserted to predict fluxes for a particular basin). All P values <0.001.

measurements of sediment concentrations. Therefore, our assessed values for Andean sediment production and the foreland basin trap efficiency are probably somewhat lower than their actual rates.

Conclusion

A new procedure is presented for mass flux analysis in large drainage basins. By separating the data set of Bolivian drainage basins into geomorphic process zones, we specifically focused attention on the process of denudation in the rapidly eroding mountainous regions. After selecting basins free from major sediment sinks and consequently from the nonphysical scaling effects of basin area, we performed a multiple regression analysis to determine the basin characteristics that best predict decadal-scale denudation rates derived from river sediment fluxes: average lithology (L) and an index for average hillslope angle (S_{avg}). That runoff is not significantly associated with modern erosion rate is both intriguing and enigmatic, although its effect may be obscured by the relationship between runoff and slope, suggesting complex feedback relationships between runoff, tectonic uplift, channel network incision, valley slope morphology, mass wasting, and sediment discharge from active orogens. Finally, to estimate sediment fluxes discharged from the Andes to the Amazon basin, we evaluated several hillslope-scale sediment flux models to develop a technique based on lithology and slope that is transferable to other basins. Simple slope-driven power and exponential models predict a flux rate of 2.3–3.1 Gt/yr from the Amazonian Andes. As better topographic and lithologic data become available, such models should become more robust and transportable.

ACKNOWLEDGMENTS

This work was supported by a NASA research grant (NAG5-6120) and an Earth Systems Science Graduate Fellowship to R. Aalto. Suggestions from W. Dietrich, P. Bierman, J. Laronne, and M. Hicks improved the manuscript.

REFERENCES CITED

Aalto, R. 1995. Discordance between suspended sediment diffusion theory and observed sediment concentration profiles in rivers. MS thesis, University of Washington, Seattle, 98 p.

———. 2002. Geomorphic form and process of mass flux within an active orogen: denudation of the Bolivian Andes and sediment transport and deposition within the channel-floodplain systems of the Amazonian foreland. PhD thesis, University of Washington, Seattle.

Aalto, R.; Dunne, T.; and Guyot, J. L. 1996. Geomorphic controls on Andean denudation rates. EOS: Trans. Am. Geophys. Union 77:46.

Aalto, R.; Maurice-Bourgoin, L.; Dunne, T.; Montgomery, D. R.; Nittrouer, C. A.; and Guyot, J. L. 2003. Episodic sediment accumulation on Amazonian floodplains influenced by El Niño/Southern Oscillation. Nature 425:493–497.

Ahnert, F. 1970. Functional relationships between denudation, relief, and uplift in large mid-latitude drainage basins. Am. J. Sci. 268:243–263.

Bliss, N., and Olsen, L. 1996. 30-arc-second digital elevation model (DEM) for South America, United States. Sioux Falls, SD, U.S. Geol. Surv. EROS Data Center.

Burbank, D. W.; Blythe, A. E.; Putkonen, J.; Pratt-Sitaula, B.; Gabet, E.; Oskin, M.; Barros, A.; and Ojha, T. P. 2003. Decoupling of erosion and precipitation in the Himalayas. Nature 426:652–655.

Burbank, D. W.; Leland, J.; Fielding, E.; Anderson, R. S.; Brozovic, N.; Reid, M. R.; and Duncan, C. 1996. Bedrock incision, rock uplift and threshold hillslopes in the northwestern Himalayas. Nature 379:505–510.

Carson, M. A., and Kirkby, M. J. 1972. Hillslope form and process. Cambridge, Cambridge University Press.

Chase, C. G. 1992. Fluvial landsculpting and the fractal dimension of topography. Geomorphology 5:39–57.

Collins, B., and Dunne, T. 1989. Gravel transport, gravel harvesting, and channel-bed degradation in rivers draining the southern Olympic Mountains, Washington, USA. Environ. Geol. Water Sci. 13:213–224.

Dunne, T.; Mertes, L. A. K.; Meade, R. H.; Richey, J. E.; and Forsberg, B. R. 1998. Exchanges of sediment between the floodplain and channel of the Amazon River in Brazil. Geol. Soc. Am. Bull. 110:450–467.

Ferguson, R. I. 1987. Accuracy and precision of methods fore estimating river loads. Earth Surf. Proc. Landf. 12: 95–104.

Finlayson, D. P.; Montgomery, D. R.; and Hallet, B. 2002. Spatial coincidence of erosional and metamorphic hot spots in the Himalaya. Geology 20:219–222.

Fournier, F. 1960. Climat et érosion: la rélation entre l'érosion du sol par l'eau et les précipitations atmosphériques. Paris, Presse Universitaire de France.

Gilbert, G. K. 1877. Report on the geology of the Henry Mountains: geographical and geological survey of the Rocky Mountain region. Washington, DC, Government Printing Office, 106 p.

Granger, D. E.; Kirchner, J. W.; and Finkel, R. 1996. Spatially averaged long-term erosion rates measured from in-situ-produced cosmogenic nuclides. J. Geol. 104: 249–257.

Quaternary palaeoclimates of the southern tropical Andes and adjacent regions. Palaeogeogr. Palaeoclimatol. Palaeoecol. 194:187–206.

Sklar, L. S., and Dietrich, W. E. 2001. Sediment and rock strength controls on river incision into bedrock. Geology 29:1087–1090.

Summerfield, M. A., and Hulton, N. J. 1994. Natural controls of fluvial denudation rates in major world drainage basins. J. Geophys. Res. 99:13,871–13,883.

Trimble, S. W. 1976. Unsteady state denudation. Science 191:871.

———. 1977. The fallacy of stream equilibrium in contemporary denudation studies. Am. J. Sci. 277:876–887.

Tucker, G. E., and Slingerland, R. L. 1994. Erosional dynamics, flexural isostasy, and long-lived escarpments: a numerical modeling study. J. Geophys. Res. 99: 12,229–12,243.

van der Beek, P., and Braun, J. 1999. Controls on post-mid-Cretaceous landscape evolution in the southeastern highlands of Australia: insights from numerical surface process models. J. Geophys. Res. 104: 4945–4966.

Walling, D. E., and Webb, B. W. 1981. The reliability of suspended sediment load data: erosion and sediment transport measurement. Int. Assoc. Hydrol. Sci. Publ. 133, p. 177–194.

———. 1983. Patterns of sediment yield. *In* Gregory, K. J., ed. Background to paleohydrology. Chichester, Wiley, p. 69–100.

Willett, S. D., and Brandon, M. T. 2002. On steady states in mountain belts. Geology 20:175–178.